Biofilm 6 (2023) 100164

Contents lists available at ScienceDirect

Biofilm

journal homepage: www.sciencedirect.com/journal/biofilm

Unravelling host-pathogen interactions by biofilm infected human wound models

Jana Wächter [1], Pia K. Vestweber [1], Viktoria Planz, Maike Windbergs [*]

Institute of Pharmaceutical Technology, Goethe University Frankfurt, Frankfurt am Main, Germany

ARTICLE INFO

Keywords:
Bacterial biofilms
In vitro skin infection model
Host-biofilm interactions
Persistent wound infections
Innate immune response

ABSTRACT

Approximately 80 % of persistent wound infections are affected by the presence of bacterial biofilms, resulting in a severe clinical challenge associated with prolonged healing periods, increased morbidity, and high healthcare costs. Unfortunately, *in vitro* models for wound infection research almost exclusively focus on early infection stages with planktonic bacteria. In this study, we present a new approach to emulate biofilm-infected human wounds by three-dimensional human *in vitro* systems. For this purpose, a matured biofilm consisting of the clinical key wound pathogen *Pseudomonas aeruginosa* was pre-cultivated on electrospun scaffolds allowing for non-destructive transfer of the matured biofilm to human *in vitro* wound models. We infected tissue-engineered human *in vitro* skin models as well as *ex vivo* human skin explants with the biofilm and analyzed structural tissue characteristics, biofilm growth behavior, and biofilm-tissue interactions. The structural development of biofilms in close proximity to the tissue, resulting in high bacterial burden and *in vivo*-like morphology, confirmed a manifest wound infection on all tested wound models, validating their applicability for general investigations of biofilm growth and structure. The extent of bacterial colonization of the wound bed, as well as the subsequent changes in molecular composition of skin tissue, were inherently linked to the characteristics of the underlying wound models including their viability and origin. Notably, the immune response observed in viable *ex vivo* and *in vitro* models was consistent with previous *in vivo* reports. While *ex vivo* models offered greater complexity and closer similarity to the *in vivo* conditions, *in vitro* models consistently demonstrated higher reproducibility. As a consequence, when focusing on direct biofilm-skin interactions, the viability of the wound models as well as their advantages and limitations should be aligned to the particular research question of future studies. Altogether, the novel model allows for a systematic investigation of host-pathogen interactions of bacterial biofilms and human wound tissue, also paving the way for development and predictive testing of novel therapeutics to combat biofilm-infected wounds.

1. Introduction

Impaired wound healing represents a major burden for today's healthcare system, as it not only significantly decreases the patients' quality of life but also has a high socio-economic impact [1]. Even worse, approximately 80 % of such wounds are affected by bacterial biofilms according to a meta-analysis of clinical studies [2]. Bacterial biofilms are characterized as persistent, structurally organized clusters of bacteria in a matrix, forming a protective shield against the host's immune defense mechanisms and fostering antimicrobial resistance [3]. Biofilm models cultivated *in vitro* on artificial surfaces have successfully been used to gain a molecular and mechanistic understanding of biofilm formation and maturation [4]. However, to understand interactions of biofilm and biological tissue for the development and testing of effective therapeutics against wound infections, both components, the biofilm and the tissue, need to be represented in a suitable model.

In vivo animal models are frequently used, with mice being the predominant species, accounting for over 70 % of the total usage in Germany [5,6]. However, particularly in wound infection studies, the translatability of murine models to the human *in vivo* situation is limited due to differences in immune response and anatomy of the skin itself [7,8]. Further, the contraction of mouse skin upon wounding caused by an additional muscle layer in rodent skin (*panniculus carnosus*) poses another problem. Additional major disadvantages comprise high costs

* Corresponding author. Institute of Pharmaceutical Technology, Goethe University Frankfurt, Max-von-Laue-Str. 9, 60438, Frankfurt am Main, Germany.
E-mail address: windbergs@em.uni-frankfurt.de (M. Windbergs).
[1] These authors contributed equally to this work.

https://doi.org/10.1016/j.bioflm.2023.100164
Received 22 September 2023; Received in revised form 19 October 2023; Accepted 20 October 2023
Available online 2 November 2023

and lacking standardization of experimental set-ups [9,10]. Against this background, the development of alternative human-based biofilm-infected wound models is of particular importance.

In general, *in vitro* wound models range from two-dimensional cell monolayers over three-dimensional tissue-engineered human skin models to human skin explants (*ex vivo* models) [11,12]. While cell monolayers offer a simple method for basic research purposes, the pathophysiology and microenvironment of human skin *in vivo* is not accurately reflected, since bacterial invasion and interaction with different cell types or the extracellular matrix cannot be mimicked [13]. Three dimensional models containing all layers of the native epidermis and dermis represent a more sophisticated approach. Briefly, they are generated by culturing dermal fibroblasts in a matrix in combination with primary keratinocytes at the air-liquid interface. Several providers offer commercially available human skin models, allowing for standardization across different laboratories [13]. Still, other features of the skin including immune cells or hair follicles are usually missing. Full human skin explants depict more native conditions, as they include all cellular elements and their interactions [9].

Different approaches for mimicking infected wounds with bacterial biofilms *in vitro*, either with tissue-engineered human *in vitro* skin models or *ex vivo* human skin biopsies, are reported in literature [14–16]. The co-cultivation of such *in vitro* human skin tissue models with bacteria is generally challenging, as cultivation media provide an excessive nutrition source for bacteria further promoting their exponential replication kinetics. This results in overgrowth of the skin tissue by bacteria as well as toxic effects on the cells, significantly reducing their viability [17]. As a bacterial biofilm requires up to several days for maturation, direct inoculation of skin tissue with bacteria and subsequent biofilm formation and maturation in direct co-culture (as performed in animal models) is impossible [18]. Nevertheless, this method is still used in *in vitro* studies for extremely limited cultivation periods without complete biofilm maturation [19–21]. Other approaches involve the separate cultivation of skin tissue and bacteria until biofilm maturation. As translocation of an intact biofilm cultivated in traditional model systems is impossible due to insufficient mechanical stability, biofilm fragments are transferred to the skin tissue [22]. However, as the complex biofilm architecture including the protective matrix significantly contributes to the overall properties of the biofilm and its resistance to antibiotics, such models unfortunately lack predictability for the situation in the human body, especially for testing of novel antibiotics. To overcome this issue, a biofilm model based on a three-dimensional fiber matrix was successfully developed, for the first time enabling the non-destructive transfer of a mature biofilm to tissue models [23].

Altogether, the number of studies conducted on *in vitro* models of biofilm-infected wounds is scarce and generally of limited predictability. In order to identify an appropriate model for future basic or translational studies in this research field, it is crucial to investigate which aspects of the biofilm-host interactions can be assessed with the different tissue models, the degree of comparability of the results and their translatability to the human *in vivo* situation. For addressing this knowledge gap, we infected human *in vitro* and *ex vivo* wound models with intact, matured *P. aeruginosa* biofilms and investigated them regarding morphology, host-pathogen interactions and the response of the wound models to biofilm infection.

2. Materials and methods

2.1. Materials

EpidermFT™ human *in vitro* skin models (antibiotic-free and antifungal-free media) were supplied by MatTek In Vitro Life Sciences Laboratories, s.r.o. (Bratislava, Slovak Republic). Gelatin (from porcine skin, 300 Bloom, type A), cellulose acetate (CA, Mn 30.000), and fetal calf serum (FCS) were purchased from Sigma-Aldrich (Steinheim, Germany). Glacial acetic acid 100 % and chloroform >99,8 % were obtained from VWR International GmbH (Darmstadt, Germany). Dulbecco's modified Eagle medium (DMEM), nutrient agar, Maxima H Minus First Strand cDNA Synthesis Kit, and *Pseudomonas aeruginosa* (*P. aeruginosa*, ATCC 27853) were purchased from Thermo Fisher Scientific GmbH (Dreieich, Germany). Dulbecco's phosphate-buffered saline (PBS) was supplied by Biowest (Nuaillé, France). Formaldehyde methanol-free 30 %, xylol >97 %, paraffin (Paraplast®), ethanol >99,8 %, eosin G 0.5 %, and hematoxylin solution according to Mayer were purchased from Carl Roth GmbH & Co. KG (Karlsruhe, Germany). Tri-Reagent was obtained by BIOZOL Diagnostica Vertrieb GmbH (Eching, Germany). Direct-zol™ RNA MiniPrep Plus Kit including DNase I Set was supplied by Zymo Research Europe GmbH (Freiburg, Germany) and PowerUp™ SYBR™ Green Master Mix was purchased from Applied Biosystems Deutschland GmbH (Darmstadt, Germany).

2.2. Preparation of human ex vivo and in vitro wound models

For the *ex vivo* models, human skin tissue was obtained from Caucasian adults, undergoing reduction surgery (Clinic for plastic and aesthetic surgery, reconstructive and hand surgery, Agaplesion Markus Krankenhaus, Frankfurt, Germany). The present study was approved by the local ethics committee (ethics commission of the state medical chamber, Hessen, 2020-1899-AF) and all skin donors gave their written informed consent. Skin explants were further processed within approximately 2 h after excision. Briefly, after removal of the subcutaneous fatty tissue, the skin tissue was either frozen at −21 °C for a minimum of 2 days, representing the status "non-viable *ex vivo* models" or immediately further processed for tissue culture to maintain viability, delineating the "viable *ex vivo* models" investigation group. To assure reproducible wounding conditions, the skin was stretched using an in-house developed device (Fig. S1) and full-thickness wounds were created by taking a standardized punch biopsy of 3 mm diameter. Subsequently, round-shaped 12 mm tissue punch samples comprising the wound surrounded by intact skin were transferred to sterile gauze soaked with DMEM +10 % FCS within a 12-well plate to allow for air-liquid cultivation and incubated overnight at 37 °C and 5 % CO_2. All experiments with *ex vivo* wound models (non-viable/viable) were conducted in triplicate with three different donors.

Commercially available *in vitro* skin models (EpidermFT™) were wounded according to the manufacturer's protocol [24]. Similar to the *ex vivo* models, wounds were created with a sterile 3 mm biopsy punch and wounded samples were incubated overnight at 37 °C and 5 % CO_2 in antibiotic-free and antifungal-free maintenance medium, provided by the manufacturer.

2.3. Preparation of biofilms and biofilm-infected wounds

Mature biofilms of *P. aeruginosa* were prepared as previously described [23]. Briefly, electrospun fiber scaffolds, equally composed of cellulose acetate and gelatin, were fabricated via blend electrospinning of a homogenous solution of both polymers in 90 % acetic acid. Process parameters for fabrication were selected according to the aforementioned publication. The electrospun scaffolds were subsequently inoculated with *P. aeruginosa* and cultivated on modified nutrient agar plates, containing 20 % FCS, at 37 °C. After 48 h cultivation, mature biofilms were used for further experiments. For wound infection, 3 mm punch biopsies of the mature biofilms were transferred onto the wound bed of the *ex vivo* and *in vitro* wound models. The infected wound models were incubated at 37 °C and 5 % CO_2 until further analysis.

2.4. Histology

Histological analysis of infected *ex vivo* wound models (non-viable/viable) was performed after 3, 6, 10, 24, and 48 h while the infected *in vitro* wound models were assessed after 3, 10, and 24 h. In parallel,

samples of uninfected, wounded models of each skin tissue condition were taken as controls and processed accordingly. Each tissue sample was fixed with 4 % phosphate-buffered formaldehyde solution for 6 h at room temperature. Afterwards, dehydration with an ascending ethanol series, clearing with xylol, and embedding in paraffin were performed, followed by the preparation of tissue cross sections measuring 5 μm in thickness using a rotary microtome (Cut 6062, SLEE medical GmbH, Nieder-Olm, Germany). In the next step, tissue sections were stained with hematoxylin according to Mayer and eosin G, following the manufacturer's protocol. Single micrographs were acquired with the bright field mode of a confocal laser scanning microscope (LSM 900, Carl Zeiss Microscopy GmbH, Jena, Germany) with the Axiocam 506 color camera (Carl Zeiss Microscopy GmbH, Jena, Germany) and a 10× objective (numeric aperture: 0.45, Plan-Apochromat, Carl Zeiss Microscopy GmbH, Jena, Germany). Subsequently, micrographs were stitched using corresponding Zeiss Zen blue software. Three samples were assessed for each condition to ensure accuracy and reliability of the results.

2.5. Raman spectroscopy

Label-free analysis of the biofilm infected *ex vivo* as well as *in vitro* skin tissues and uninfected controls was performed by recording Raman spectra at 24 h of cultivation based on the identical paraffin-embedded wound tissue samples as used for histological analysis. Tissue cross sections measuring 24 μm in thickness were mounted onto CaF_2 glass slides followed by a deparaffinization step using a descending xylol/ethanol series. The dry samples were analyzed using a WITec alpha 300R$^+$ microscope (WITec GmbH, Ulm, Germany) coupled with a 532 nm diode laser, which was adjusted to a power of 3.0 mW in front of the objective (50×, numeric aperture: 0.8, EC Epiplan-Neofluar, Carl Zeiss Microscopy GmbH, Jena, Germany). Raman spectra of the dermis and the epidermis of infected and uninfected wounded models were recorded with an integration time of 0.5 s and 10 accumulations and a spectral resolution of 4 cm^{-1} in a range of 400–3700 cm^{-1}. Background subtraction of the spectra was performed using WITec Project Plus software (WITec GmbH, Ulm, Germany), the subsequent preprocessing (normalization and cosmic ray removal) as well as the multivariate data analysis were conducted in MATLAB (Version R2023a, MathWorks, USA).

2.6. Quantification of colony forming units (CFUs)

To determine the colony forming units (CFUs) of *P. aeruginosa*, punch biopsies with a diameter of 6 mm were taken from the infected *ex vivo* wound models after 3, 6, 10, 24, and 48 h of incubation, and from infected *in vitro* wound models after 3, 10, and 24 h of incubation. The samples included the entire biofilm-infected wounds and surrounding tissue. The skin samples were placed in centrifuge tubes filled with zirconia beads (1.4–1.6 mm) and homogenized with a bead mill homogenizer (Bead Mill MAX, VWR International GmbH, Darmstadt, Germany). Aggregates of bacteria were disrupted with sonication for 2 min to obtain a single cell suspension of *P. aeruginosa*. Subsequently, serial 10-fold dilutions were prepared with sterile PBS and plated on nutrient agar plates. Visible colonies were counted after 24 h incubation at 37 °C. The experiments were performed in triplicate.

2.7. Scanning electron microscopy (SEM)

For visualization of the biofilm morphology and the host-pathogen interface as represented by the wound bed after biofilm removal, samples of infected viable and non-viable *ex vivo* wound models were collected and fixed as described above. After dehydration using an ascending ethanol series, tissues were divided in half and biofilms were detached from one section to reveal the infected wound bed. Following complete ethanol removal by critical point drying (Leica EM CPD300 Automated Critical Point Dryer, Leica Mikrosysteme GmbH, Vienna, Austria), the samples were mounted on carbon tapes and sputter-coated with gold/palladium (80 %/20 %) for 3 min (SC7620, Quantum Design GmbH, Darmstadt, Germany). Micrographs were acquired at a magnification of 2,000× and an acceleration voltage of 8 kV using a scanning electron microscope (EVO 10, Carl Zeiss Microscopy GmbH, Jena, Germany) at room temperature.

2.8. Analysis of cytokine gene expression

For determining the gene expression of the selected cytokines and chemokines IL-1β, IL-6, IL-8, and TNFα via RT-qPCR, 3 mm biopsy punches of the infected wounds were obtained from viable *ex vivo* models after 3, 6, 10, and 24 h and from *in vitro* models after 3, 10, and 24 h. As controls, samples of uninfected wound models were taken at the mentioned time points, accordingly. Immediately after collection, the tissue pieces were snap-frozen in liquid nitrogen and stored at −80 °C until further processing. Prior to RNA isolation, samples were placed in Tri-Reagent and homogenized with zirconia beads (2.8 mm) using a bead mill homogenizer (Bead Mill MAX, VWR International GmbH, Darmstadt, Germany). Furthermore, samples were washed with chloroform to optimize RNA yield and purity [25]. Total RNA was isolated using the Direct-zol™ RNA MiniPrep Plus Kit, following the manufacturer's instructions. To impede contamination with genomic DNA, digestion with DNase was also performed. The final RNA concentration was determined using the NanoQuant plate in combination with a microplate reader (Spark multimode microplate reader, Tecan, Männerdorf, Switzerland). RNA was stored at −80 °C until cDNA synthesis, where 100 ng RNA was transcribed using the Maxima H Minus First Strand cDNA Synthesis Kit. Notably, solely oligo $(dT)_{18}$ primers were applied in order to exclusively transcript eucaryotic mRNA and avoid bacteria-derived cDNA production. cDNA was quantified as already described for total RNA and stored at −80 °C. RT-qPCR experiments were performed with the PowerUp™ SYBR™ Green Master Mix, according to the manufacturer's protocol, on a Real-Time PCR System (StepOnePlus, Applied Biosystems Deutschland GmbH, Darmstadt, Germany). The applied gene-specific primer sequences are listed in Table 1 (generated with primer-blast, National Center for Biotechnology Information, NCBI). Relative gene expression was assessed by normalizing to GAPDH, relating the Ct values to the corresponding uninfected control and determining fold changes according the $2^{-\Delta\Delta Ct}$ method described by Livak and Schmittgen [26]. For each infected wound condition and time point, three samples were assessed.

2.9. Statistical analysis

CFU data is shown as mean ± standard deviation, calculated with Microsoft Office Excel. For RT-qPCR data, error bars were calculated according to Livak and Schmittgen [26] and statistical analyses were carried out based on ΔCt values. Two-tailed unpaired student-T tests were performed using Microsoft Office Excel for all statistical evaluations. The results were considered statistically significant when $p < 0.05$ (*$p < 0.05$, **$p < 0.01$, ***$p < 0.001$).

Table 1
Primers for RT-qPCR.

PRIMER	SEQUENCE (5'→ 3')
GAPDH	forward: CGGGAAGCTTGTCATCAATGG reverse: GGCAGTGATGGCATGGACTG
IL-1B	forward: AGCTACGAATCTCCGACCAC, reverse: CGTTATCCCATGTGTCGAAGAA
IL-6	forward: ACTCACCTCTTCAGAACGAATTG reverse: CCATCTTTGGAAGGTTCAGGTTG
IL-8	forward: GAGAGTGATTGAGAGTGGACCAC reverse: CACAACCCTCTGCACCCAGTTT
TNFA	forward: CCTCTCTCTAATCAGCCCTCTG reverse: GAGGACCTGGGAGTAGATGAG

3. Results

3.1. Histological characterization of biofilm-infected 3D wound models

After inoculation with mature *P. aeruginosa* biofilms, non-viable and viable *ex vivo* as well as viable *in vitro* models and their respective controls were subjected to histological characterization based on hematoxylin and eosin staining with particular focus on structural appearance and host-pathogen contact after biofilm infection. The images presented in Fig. 1 are representative for three samples analyzed for each condition.

To assure adequate tissue integrity before biofilm infection, uninfected tissue samples of all three wound model types were analyzed regarding their three-dimensional morphological appearance and structural intactness. In all three wound models, well-defined epidermal and dermal layers were observed. Furthermore, no signs of cell deformation or tissue disruption due to the freeze-thawing process were detected in the non-viable *ex vivo* skin. A remarkable difference between the *in vitro* and *ex vivo* models was noticed in thickness and structure of the dermis. While the *ex vivo* dermis reached a thickness of up to 5000 μm, the *in vitro* dermis showed a maximum thickness of 750 μm and appeared more homogeneous and denser. The wound size slightly varied, both within and between the different models.

For the viable *ex vivo* and *in vitro* models, wound healing in form of re-epithelialization occurred (Fig. 1B and C). While the wounded area of the *in vitro* model was completely re-epithelialized after 24 h, wound healing in the *ex vivo* model was limited to an epithelial tongue reaching into the wound bed.

The images obtained from the infected models revealed close contact between the biofilm and the wound bed for all models with an increase in biofilm density over time. Disruption of the tissue structure became apparent after 10 h in all models. Specifically, the *stratum corneum* constituting the uppermost layer of the human skin was detached from the skin due to partial epidermolysis. This effect further intensified in the remaining observation period.

3.2. Quantification of biofilm growth behavior in dependency of host-pathogen interactions

To assess the impact of direct host-pathogen interactions of the different wound models on the bacterial growth behavior, quantification of CFUs was performed after inoculation with mature *P. aeruginosa* biofilms, comprising approximately $4.5*10^8$ viable bacteria. Infected *ex vivo* as well as *in vitro* wound models were investigated after 3, 6, 10, and 24 h or 3, 10, and 24 h, respectively (Fig. 2A). In the case of non-viable *ex vivo* models, the number of *P. aeruginosa* steadily increased up to $6.3*10^8$ ($\pm 1.8*10^8$) bacteria per wound after 10 h, followed by a stationary phase. The results for the viable *ex vivo* and *in vitro* models revealed a significant decrease in bacterial viability at 3 h (Fig. 2B), with CFUs dropping to $2.8*10^8$ ($\pm 4.6*10^7$) and $2.0*10^8$ ($\pm 1.5*10^7$), respectively. However, bacterial counts increased thereafter. Notably, for the viable *ex vivo* models, the number of CFUs exceeded the starting value already after 6 h with $4.9*10^8$ ($\pm 1.1*10^8$) bacteria per wound. By 24 h, the number of CFUs was comparable to that of the non-viable *ex vivo* models. In contrast, the bacterial count remained lower for the biofilm-infected *in vitro* models, reaching $4.7*10^8$ ($\pm 7.3*10^7$) CFUs after 24 h.

3.3. SEM analysis of biofilm morphology and bacterial growth patterns influenced by model viability

The growth and colonization patterns of *P. aeruginosa* biofilms on viable and non-viable *ex vivo* wound models were additionally examined by SEM in order to determine the effect of model viability on the interactions with biofilm bacteria. Micrographs of the biofilms and the wound beds after biofilm removal were obtained at different time points (after 3, 6, 10, and 24 h), as shown in Fig. 3. After 3 h, a homogenous and dense bacterial growth was observed for all biofilms, independent of the underlying wound model. At this time point, nanofibers of the electrospun scaffolds were still visible. Over time, the biofilms appeared denser, with no discernible differences between the two wound models. After removal of the biofilms, imprints of electrospun fibers on the wound beds became visible in bacteria-free areas. Already after 3 h incubation, all wounds were colonized by individual bacteria, which began to form colonies from 6 h. By 10 h, bacterial growth patterns varied considerably between the two models. On viable excised skin, extensive colonization and the formation of larger aggregates were observed (Fig. 3A). In contrast, significantly fewer bacteria were present on the wound beds of non-viable *ex vivo* models, mostly growing as individual cells (Fig. 3B).

3.4. Investigation of the model composition and changes induced by biofilm infection using Raman spectroscopy

Raman spectra were collected from cross sections of infected and uninfected models after 24 h of cultivation. Differences in the tissue composition between the wound models, as well as in response to the biofilm infection on a molecular level were assessed. For the analysis of the viable and the non-viable *ex vivo* model, samples of the same donor were selected, respectively. Spectra were acquired in the wounded area from the remaining epidermis and dermis of the infected models and compared to spectra obtained from the *stratum corneum*, the viable epidermis and dermis of the uninfected control models.

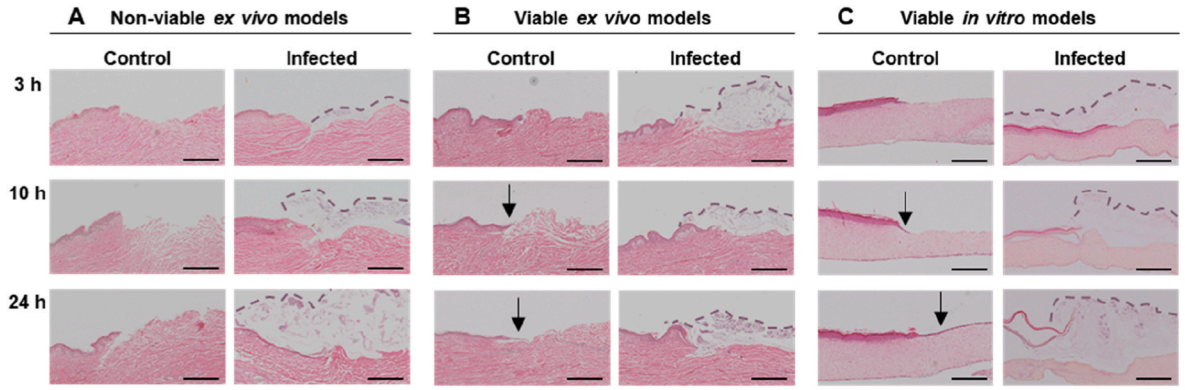

Fig. 1. Representative brightfield images of hematoxylin & eosin-stained paraffin sections of uninfected controls and infected wound models: (A) non-viable *ex vivo* models, (B) viable *ex vivo* models, and (C) *in vitro* models. Infected wound models were inoculated with mature *P. aeruginosa* biofilms and samples for histological analysis were collected after 3, 10, and 24 h incubation period. *P. aeruginosa* biofilms are bordered with dashed lines as guide to the eye and arrows indicate areas of re-epithelization. Scale bar = 500 μm.

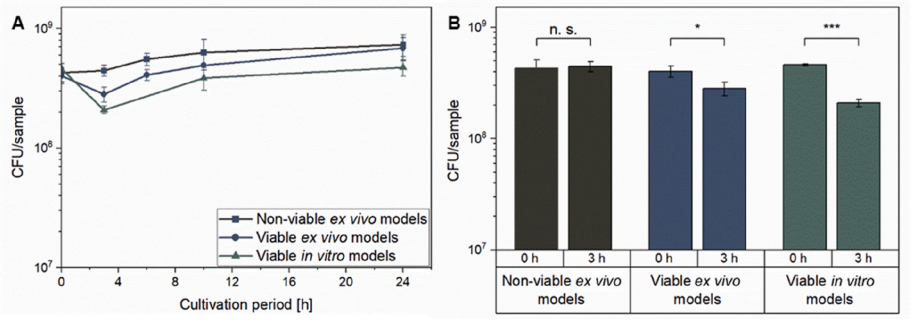

Fig. 2. Evaluation of colony forming units (CFUs) to monitor bacterial growth of *P. aeruginosa* on viable *ex vivo* models, non-viable *ex vivo* models, and viable *in vitro* models of human wounds. (A) CFUs were determined at 0, 3, (6), 10 and 24 h after infection with mature biofilms. (B) The changes in viable bacterial counts from 0 to 3 h were statistically evaluated using two-tailed unpaired student T tests with *p < 0.05, **p < 0.01, ***p < 0.001. All results are shown as mean with standard deviations and all experiments were conducted in triplicate.

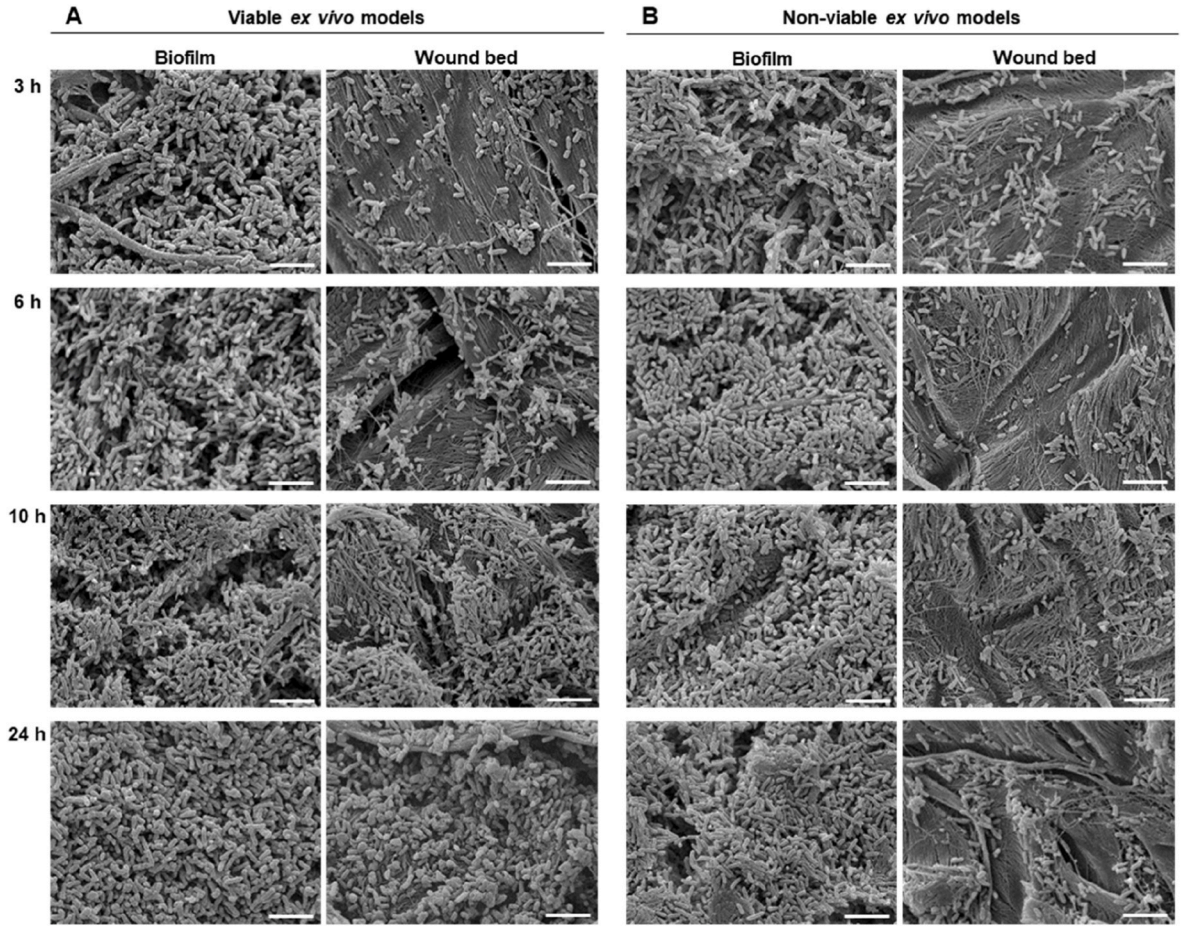

Fig. 3. Assessment of biofilm morphology and bacterial growth pattern on wound beds after biofilm removal using scanning electron microscopy (SEM). (A) Viable *ex vivo* wound models as well as (B) non-viable *ex vivo* wound models were infected with *P. aeruginosa* biofilms and cultivated for 3, 6, 10 and 24 h prior to SEM analysis. A magnification of 2,000× and an acceleration voltage of 8 kV were applied. Scale bar = 5 μm.

The Raman spectra of the epidermal regions primarily exhibited Raman signals associated with proteins and lipids (Fig. 4A). In detail, Raman signals at 1008 cm^{-1}, 1444 cm^{-1}, and 1650 cm^{-1} represented the vibrational modes of aromatic amino acids, the deformation of C–H bonds and the carbonyl group (C═O) vibration of amide I, respectively [27,28]. Additional signals observed at 1134 and 1300 cm^{-1} were attributed to the vibration of C–C bonds of lipids with skeletal trans conformation and the deformation of C–H2 bonds of lipids [27]. C–H stretching modes, corresponding to lipid alkyl chains, were assigned to signals in the range of 2850–2950 cm^{-1} [29]. The Raman spectra of the dermal regions are additionally characterized by two double peaks at 850 to 880 cm^{-1} and 920 to 950 cm^{-1}, corresponding to C–C stretching of the protein backbone and the proline/hydroxyproline ring of collagen, and a distinct signal at 1246 cm^{-1}, representing the C–N stretching of amide bonds (Fig. 4B) [30].

The differences between the *ex vivo* and the *in vitro* models, as well as between the respective infected and uninfected models, were assessed using principal component analysis (PCA). The PCA was independently conducted with the epidermal spectra and the dermal spectra. Subsequent Pareto plots revealed that three principal components (PCs)

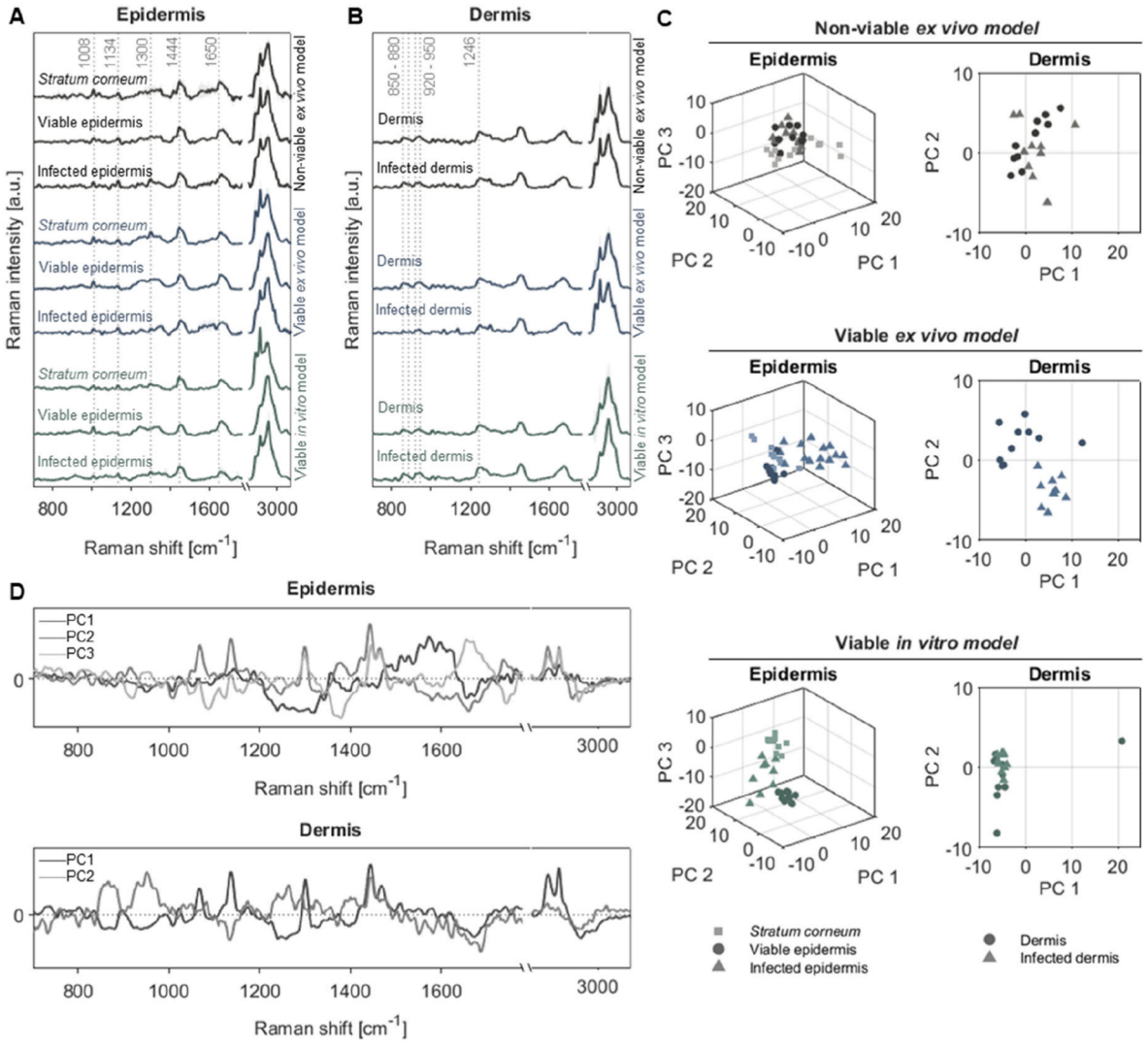

Fig. 4. Investigation of the tissue composition of the human-derived wound models and their response to biofilm infection after 24 h using Raman spectroscopy. (A) Mean spectra of the *stratum corneum*, the viable epidermis and the infected epidermis and (B) the dermis and the infected dermis of the viable and the non-viable *ex vivo* model as well as the viable *in vitro* model. (C) Score plots of the principal component analysis of the epidermal and the dermal spectra and (D) corresponding loading plots.

explained more than 50 % of the total variability of the epidermal spectra (PC 1: 26.3 %, PC 2: 14.4 %, PC 3: 10.3 %), while two principal components explained more than 50 % of the total variability of the dermal spectra (PC 1: 39.0 %, PC 2: 12.1 %) (Fig. S2). For clarity, the scores of the different models were plotted separately (Fig. 4C). The score plots of the epidermal spectra indicated that the *stratum corneum*, the viable and the infected epidermis can be distinguished on the basis of their Raman signals in case of the viable *ex vivo* model and the *in vitro* model. However, no clear separation of the groups was apparent for the non-viable *ex vivo* model. Further, compared to the *in vitro* model, both *ex vivo* models exhibited greater variability in the Raman spectra. The latter observation also applied to the score plots of the dermal spectra. Despite of the signal heterogeneity, distinct clusters of Raman spectra of the infected and uninfected samples were observed for the viable *ex vivo* model. In contrast, neither the score plot of the non-viable *ex vivo* model nor that of the *in vitro* model exhibited a clear separation of the dermal spectra.

The PC loading plots revealed discriminant wavenumbers, reflecting different components of the tissue analyzed (Fig. 4D). Epidermal samples with a positive PC 1 score were correlated with an increase of the amide II signal, conversely, a negative PC 1 score indicated an elevated amide III signal. PC 2 was assigned to the relation of lipids (positive scores) to proteins (negative score), while PC 3 depicted the ratio between overall protein (positive score) and DNA Raman signals (negative score). Regarding the PCA of the dermal spectra, a positive PC 1 score was associated with lipids, whereas proteins were reflected by a negative PC 1 score. Differences in the collagen composition of the tissues were visualized by PC 2 (positive score). A full peak assignment can be found in the supporting information (Table S1).

3.5. Evaluation of cytokine gene expression representing pro-inflammatory mediators of the immune response

To analyze the innate immune response of the different wound models to the biofilm infection, the time-dependent gene expression of selected pro-inflammatory cytokines and chemokines, namely IL-1β, IL-6, IL-8, and TNFα, was evaluated in viable *ex vivo* and *in vitro* skin wound models infected with *P. aeruginosa* biofilms after 3, 6, 10, and 24 h or 3, 10 and 24 h, respectively. The RT-qPCR results of biofilm-infected *ex vivo* wound models are shown in Fig. 5A. In the case of IL-1β, already after 3 h high expression levels of 12.7 (±12.6) could be observed, even though this increase in fold changes was not statistically significant.

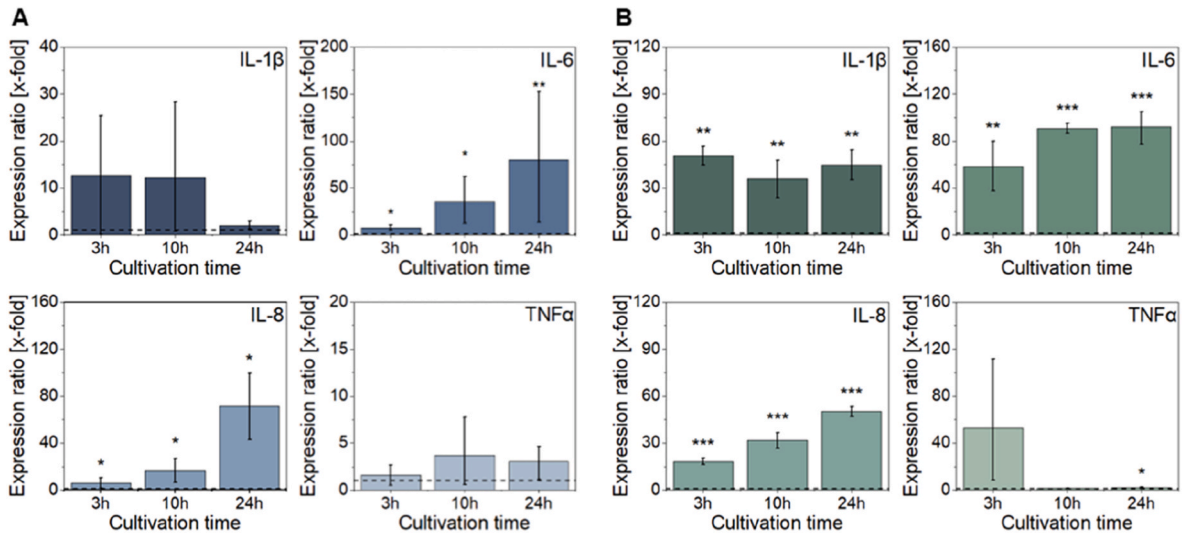

Fig. 5. Gene expression of pro-inflammatory cytokines in response to biofilm infection by RT-qPCR. (A) Viable *ex vivo* wound models as well as (B) *in vitro* wound models were infected with mature *P. aeruginosa* biofilms and gene expressions of IL-1β, IL-6, IL-8, and TNFα were determined after 3, 10, and 24 h cultivation. The dashed line indicates a fold change of 1. The mean expression ratio and error bars were calculated according to the $2^{-\Delta\Delta Ct}$ method [31]. For statistical analysis, two-tailed unpaired student T tests based on ΔCt values was performed, comparing the infected samples with the corresponding uninfected control (*$p < 0.05$, **$p < 0.01$, ***$p < 0.001$).

Notably, the lowest expression levels were found after 24 h incubation. For IL-6 and IL-8, RT-qPCR results revealed significantly higher gene expression levels during biofilm infection compared to the uninfected control for all time points examined. While the upregulation of IL-6 was already pronounced after 10 h reaching fold changes of 35.2 (+26.9/−23.1) and remained relatively stable thereafter, gene expression of IL-8 peaked at 24 h with fold changes of 71.2 (±28.2) after showing low levels at the previous time points. Throughout the study, only low gene expressions of TNFα were observed compared to the control with fold changes reaching from approximately 1.5 to 3.7. In general, high standard deviations were revealed for the experiments conducted with *ex vivo* wound models. For experiments with the *in vitro* wound models, RT-qPCR results are shown in Fig. 5B. Gene expressions of biofilm-infected *in vitro* skin wounds showed similarities in cytokine expression after 3, 10 and 24 h of biofilm infection compared to the *ex vivo* skin. IL-1β, IL-6, and IL-8 were significantly upregulated at all time points upon infection. While for IL-1β and IL-6 high and stable fold changes were obtained over the total investigated period with maximal values of 50.5 (±5.9) and 92.0 (±14.8), respectively, IL-8 expression rose over time and reached a maximal fold change of 50.3 (±3.3) after 24 h. Again, minimal upregulation of TNFα was observed for the later time points, while high fold changes of 52.8 (±44.4) occurred after 3 h. With a few exceptions, standard deviations were low for the experiments with the commercially available *in vitro* skin models.

4. Discussion

In the past, *in vitro* biofilm models cultivated in artificial environments were crucial for obtaining valuable fundamental molecular and mechanistic insights into the formation and maturation of bacterial biofilms, but unfortunately, certain limitations persist as they fail to reflect the interaction of biofilm and biological tissue present in the complex *in vivo* scenario [32]. Understanding this interplay is essential for the rational development and testing of effective therapeutics against wound infections. Consequently, it is imperative to create a suitable model that represents both components, the biofilm and the affected tissue. While it is ethically impossible to include humans in preclinical biofilm-related wound infection studies, the utilization of animal test models also poses several significant drawbacks including limited predictability to the human *in vivo* situation, due to substantial interspecies differences in structural composition as well as in immune and wound healing mechanisms [7,8]. Against this background, an urgent need for predictive alternative human-based infection models becomes evident. Yet, the accurate imitation of the biofilm-infection state of wound infections *in vitro* remains challenging, due to detrimental effects of relevant bacteria on the host tissue during biofilm maturation [18]. Consequently, current human-derived *in vitro* infection models mainly focus on the sole replication of the initial infection phase caused by planktonic bacteria, while assessment of more advanced infection stages with biofilm formation and corresponding host-pathogen interactions still depend on animal models. To cover this gap, a mature biofilm model based on an electrospun scaffold was developed, which can be transferred to *in vitro* tissue models without destruction [23]. In this study, a comparative approach of biofilm-infected wound models was employed by combining mature biofilms with different human *ex vivo* and *in vitro* wound models of varying complexity. A pre-cultivation period of 48 h was selected to attain biofilm maturity, which was previously verified by the emergence of crucial structural and functional biofilm characteristics [23]. Simultaneously, the cultivation separately from the wound tissue was kept as short as possible to minimize the potential influence of abiotic elements of the *in vitro* setting on biofilm development. For the first time, intact and mature *P. aeruginosa* biofilms were used to induce advanced infections on wounded human *ex vivo* skin models (viable and non-viable) as well as on commercially available human *in vitro* skin models (EpidermFT™, MatTek In Vitro Life Sciences Laboratories, s.r.o). The infected wound models were subsequently investigated regarding morphology, host-pathogen interactions and the response of the wounded skin tissue to biofilm infection. This comprehensive analysis aimed at assessing the translatability of these models to the human body, while simultaneously identifying appropriate application fields for the different models under investigation.

Based on histochemical analysis of the infected and uninfected models, detailed information in terms of morphological tissue characteristics and structural changes induced by biofilm infection could be attained. Each wound model comprised the complex three-dimensional and hierarchically structured morphology of human skin characterized by a multi-layered epidermis with a cornified top-sheet and an underlying dermal compartment. Adverse effects on tissue integrity of the non-viable ex *vivo* models following freezing at −20 °C and subsequent thawing could not be observed, which is in good accordance with the

literature [19]. This represents a non-negligible aspect, as tissue integrity loss during model preparation impedes the identification of destructive effects caused by bacterial biofilms. Accordingly, these findings corroborated the general applicability of freeze-thawed wound models for evaluation of structural changes during infection. Differences in thickness and structural complexity of the dermal compartment between the *ex vivo* and *in vitro* models could affect the spatial-temporal penetration behavior of bacteria and nutrients. However, visible differences in terms of bacterial invasion were not apparent. In addition, no adverse impact on epidermal-dermal cross-communication as mandatory key event for re-epithelialization could be detected, as visualized by pronounced epithelial tongue formation sprouting from the wound edges into the wound bed. As previously reported, the altered dermal structure in *in vitro* models does not hinder cellular key interactions required for proper wound healing [33]. Re-epithelialization as indicator for skin viability was observed in both, viable *ex vivo* and *in vitro* control models, confirming a wound healing mechanism comparable to the human *in vivo* situation, in contrast to murine models, where excisional wounds predominantly close by tissue contraction [8]. Confirming previous findings, the analysis of the infected models revealed adequate biofilm attachment to the wound bed, thereby promoting optimal conditions for host-pathogen interactions at the biofilm-tissue interface [23]. Hence, each tested wound model was suitable to mimic the close contact between biofilm and tissue, thus being capable of recapitulating the *in vivo* situation. The histological analysis further unveiled epidermolysis in all three infected models, characterized by the loss of keratinocytes and detachment of the epidermis from the underlying tissue, which is in line with literature knowledge [9,34]. Notably, this effect occurred in both, viable and non-viable models, suggesting that the defense mechanisms of viable skin cells were not sufficient to effectively combat biofilm-induced tissue disruption. From a histological perspective, all tested biofilm-infected wound models served as suitable alternatives to animal testing if studying structural aspects is of interest. In this context, commercial *in vitro* models can be advantageous due to greater availability in case of limited access to excised tissue. Further, non-viable *ex vivo* models are an appropriate choice if the expertise to maintain skin viability during culture is lacking.

Quantitative monitoring of the *P. aeruginosa* biofilm growth on the different wound models was assessed by CFUs analysis. Results from infected, non-viable *ex vivo* wound models were in accordance with typical, unhindered bacterial growth behavior in a nutrient-rich environment, characterized by an initial exponential growth interval followed by a stationary phase. These findings aligned with existing literature that supports the notion of *P. aeruginosa* providing various strategies for utilizing skin compounds as a source of nutrient supply to promote bacterial growth [35,36]. Additionally, the lack of active defense mechanisms against bacterial growth within the non-viable models allows for unhindered bacterial growth. Interestingly, bacterial growth was initially impeded on infected viable wound models resulting in reduced numbers of viable *P. aeruginosa* at 3 h. This effect was particularly pronounced for the *in vitro* wound models. Since these models lack immune cells, the observed defense mechanism was predominantly originating from resident skin cells, such as keratinocytes and fibroblasts. In this context, one important component of the first-line defense cascade in response to bacterial infection is the production of antimicrobial peptides (AMPs), particularly by epithelial cells [37]. AMPs produced by human keratinocytes have been shown to exhibit antibacterial activity against *P. aeruginosa* in both, planktonic and biofilm phenotypes, and thus may contribute to the observed significant loss of bacterial viability in early infection [38,39]. Detection of such effects using animal models is restricted due to interspecies differences in the quantity and variety of AMPs [40]. In the *ex vivo* models, an additional effect of active immune reactions by immune cells was conceivable. However, complete eradication of bacterial biofilms was not observed due to e.g., the lack of a vascular system, restricting adaptive immune mechanisms [41]. In all *in vitro* and *ex vivo* models, biofilms were able to recover and to persist, resulting in biofilm-related, advanced states of wound infections. The slightly reduced number of viable *P. aeruginosa* bacteria observed on *in vitro* models after 24 h could be attributed to a reduced supply with nutrients due to their denser dermis structure impeding diffusion. Furthermore, the composition of the collagen matrix might affect its degradation and metabolization by bacteria.

The CFU analysis demonstrated that inoculation with mature *P. aeruginosa* biofilms resulted in a manifest wound infection on all tested models, since, at all time points, the total bacterial load exceeded the critical level of 10^5 bacteria/g tissue, indicating manifest tissue infections [42]. For a detailed view, SEM micrographs of the biofilms and of the underlying wound beds were acquired for viable and non-viable *ex vivo* models. Consistent with previous reports, the biofilms were characterized by a homogenous bacterial distribution including dense aggregates on the nanofiber scaffolds [23]. Biofilm density steadily rose during the incubation time, without reflecting the initial reduction in bacterial viability on viable wound models observed by CFU analysis. This can be attributed to captured dead bacteria in the biofilm matrix being not distinguishable from viable ones by SEM visualization. While no significant differences in bacterial growth patterns within the biofilms were detected among the two wound models, variations in bacterial growth behavior on the wound beds were apparent, depending on the viability status of the models. After 24 h, the formation of microcolonies in the wound beds of viable *ex vivo* models was consistent with the reported growth patterns of biofilms in clinical samples of human chronic wound infections [43,44]. Consequently, the predominant presence of individual bacteria in the wound beds of non-viable *ex vivo* models did not properly represent the *in vivo* situation. Previous literature suggests that multiple factors may contribute to this phenomenon. Kirketerp-Møller et al. assumed that single bacteria cannot withstand the hosts' immune responses, thus, the presence of active immune mechanisms forces the bacteria to form microcolonies protecting them against external attacks [44]. The presence of pro-inflammatory cytokines may also be relevant serving as stimulus for growth and biofilm formation of *P. aeruginosa* [45,46]. Even though general biofilm growth appeared similar on all wound models, our findings highlight the importance of considering the wound viability status when investigating the pathogenesis of biofilm infections regarding biofilm-host interactions.

Furthermore, confocal Raman microscopy was applied to gain deeper insights into biofilm-host interactions at a molecular level, influenced by differences in wound model composition. With its non-invasive and chemically selective working principle, Raman microscopy allowed for a detailed analysis of tissue components without the need of labelling. Raman spectra of epidermal and dermal regions revealed chemically selective fingerprint peak patterns, containing information about the tissue composition, the structure of single molecules as well as the dynamics and interactions between different molecules. The peaks observed for the epidermal (represented by keratin) and the dermal (represented by collagen) compartment of the uninfected control models were overall consistent with previous studies [47,48]. However, the comparison of the models revealed varying peak ratios, suggesting distinct differences in the composition of the tissue models. The spectra of the two viable models showed similarities and reflected the terminal differentiation of keratinocytes in the viable part of the epidermis to corneocytes in the upper *stratum corneum* based on a decrease in DNA-derived and a simultaneous increase in protein-related Raman signals. No comparable findings were observed for non-viable *ex vivo* models. This can be attributed to the fact that the keratinocytes already died during the freezing process of the wound model for storage at −20 °C. In the case of the dermal spectra, the *in vitro* model differed from both *ex vivo* models due to a decreased variability in the spectra regarding the lipid/protein ratio, corresponding to the homogenous appearance of the samples in the histological analysis. In a previous study, Ali et al. also applied Raman microscopy on tissue sections of human skin and the EpidermFT™ *in vitro* model, reporting comparable

spectra of the epidermal and dermal layers [49]. To evaluate the response to the biofilm infection, the spectra of the infected skin layers were compared to the corresponding uninfected control. Close similarities between the spectra obtained from the infected and uninfected epidermal layers of non-viable *ex vivo* model can again be explained by the prior cell death during freezing. In contrast, the viable *ex vivo* model exhibited the bacterial damage of the epidermis by a decreased DNA Raman signal, which was comparable to the spectrum of the *stratum corneum*. Additionally, the variability in the lipid/protein ratio increased, which also applied to the infected epidermis of the *in vitro* model. However, while the spectrum of the viable *ex vivo* model is shifted towards a higher lipid signal, the spectrum of the *in vitro* model moved towards an increased protein signal. This difference was attributed to the fact that the epidermis of the *in vitro* model consisted exclusively of keratinocytes, whereas the epidermis of the excised human skin is more complex and additionally contained other cell types [49]. While for the dermal regions, no clear separation of the spectra groups was observed for the non-viable *ex vivo* model, dermal spectra of the viable *ex vivo* model showed a decrease of the collagen signal, indicating that collagen served as a nutrient source for bacteria. These pronounced changes were absent in the dermis of the *in vitro* model, supporting together with the differences in the lipid/protein ratio the hypothesis that compositional differences lead to a potentially reduced nutritional role compared to the *ex vivo* model. Thus, for investigating compositional changes of the wounded tissue upon biofilm infections at a molecular level, viable wound models proved to be particularly appropriate compared to the non-viable counterparts. Moreover, while *ex vivo* models exhibited a more complex composition and a closer similarity to the *in vivo* conditions, the advantage of commercial *in vitro* models lied in the lower variability.

In a next step, viable wound models (*ex vivo/in vitro*) were assessed regarding their capability to evoke an *in vivo*-like human innate immune response induced by *P. aeruginosa* biofilm infection. Analysis of non-viable *ex vivo* models was not conducted due to the absence of active defense mechanisms. Gene expression profile of certain pro-inflammatory cytokines (IL-1β, IL-6, TNFα) and a chemokine (IL-8) were evaluated as these pro-inflammatory mediators play a significant role in the immune response during acute and chronic wound infections [50–52]. Chronic wound infections, mostly biofilm-related, are generally associated with a prolonged inflammatory phase exhibiting persistent high levels of pro-inflammatory cytokines [52]. The initial upregulation of IL-1β, a crucial early-phase cytokine, is in line with literature und could be demonstrated for both viable model settings [53]. In contrast, the reduction of IL-1β gene expression after 24 h in the *ex vivo* models deviated from initial expectations for advanced, biofilm-related wound infections. However, it has been previously described that *P. aeruginosa* provides different immunomodulating mechanisms, impeding the production of pro-inflammatory cytokines including IL-1β [54,55]. The reasons why this effect is solely observed in *ex vivo* models remain not fully understood, probably due to the absence of immune cells, especially macrophages, in *in vitro* models [56]. For both wound models, the observed high fold changes of IL-6 after 10 h (early phase of infection), up to 24 h (persistent infection) were consistent with previous *in vivo* reports [53,57,58]. The detected time-delayed increase in IL-8 expression can be attributed to its dependency on the prior expression of other cytokines, in particular IL-1β and TNFα [59]. The pro-inflammatory cytokine TNFα is reported to be extensively secreted during the early phase of skin inflammation, followed by a rapid down-regulation thereafter [53]. In this study, an early up-regulation could only be observed in case of *in vitro* models. For all subsequent time points, the gene expression remained consistently low, thus mirroring *in vivo* observations. Overall, both, *ex vivo* and *in vitro* models exhibited similar patterns of cytokine gene expression dynamics, aligning with literature reports on human *in vivo* skin inflammation upon bacterial infection. The *ex vivo* models incorporating various cell types capable of cytokine production including resident immune cells and non-immune skin cells (e.g., keratinocytes and fibroblasts). A limited number of studies on immune response within infected *ex vivo* wound models exists, reporting elevated levels of pro-inflammatory cytokines upon infection, as also observed in the present study [9,60]. In contrast, commercially available in *vitro* models are characterized by their lack of harboring any immune cells. Nevertheless, these *in vitro* models demonstrated high levels of pro-inflammatory cytokines, highlighting the significant role of non-immune skin cells contributing to the innate skin immunity [50,61]. Previous *in vitro* studies using biofilm-conditioned media, demonstrated increased gene expression of pro-inflammatory cytokines [62,63]. Further, data derived from *ex vivo* models revealed high standard deviations due to a pronounced inter-individual variability, thus restricting reproducibility. Experiments conducted with commercially available *in vitro* models showed a high level of reproducibility due to their well-defined standardization in terms of model composition. Thus, the applicability of both viable wound models could be proven for studying host immune responses to mature biofilm infections even though differing in immune complexity.

In the present study, we identified the distinct strengths and advantages of biofilm-infected human three-dimensional *ex vivo* and *in vitro* wound models differing in biological complexity, accompanied by exploring the limitations of each model dependent on the scientific question of interest. The applicability of each presented wound model for common investigation purposes encompassing the determination of bacterial growth and the structural appearance could be verified to be independent of tissue viability status. However, we strongly recommend the use of viable models, especially, when direct biofilm-skin tissue interactions are of major interest. Due to a notable biological complexity of biofilm-infected e*x vivo* wound models, results derived from these test settings possess a high predictive power for translation into a clinical setting. Hence, they are particularly suitable in the context of fundamental research questions with focus on the multicellular interplay in a complex, three-dimensional environment, thus paving the way for identification of new drug targets and site-specific delivery strategies for anti-infective therapy. Commercially available *in vitro* models provide precisely controlled tissue conditions including a well-defined compositional architecture, thus being superior when a high degree of standardization and reproducibility are crucial factors, such as comparative drug screening studies. In conclusion, our findings corroborate the great potential of the three-dimensional biofilm-infected human wound models to be used across various application fields spanning from fundamental to translational research purposes.

Funding

Funding was provided by Stiftung zur Förderung der Erforschung von Ersatz-und Ergänzungsmethoden zur Einschränkung von Tierversuchen (set) (Grant number: P-070) and Deutsche Forschungsgemeinschaft (DFG, German Research Foundation) (project number 414985841). This study was supported by the Cluster project ENABLE funded by the Hessian Ministry for Science and the Arts.

CRediT authorship contribution statement

Jana Wächter: Methodology, Validation, Investigation, Formal analysis, Writing – original draft, Writing – review & editing, Visualization. **Pia K. Vestweber:** Methodology, Validation, Investigation, Formal analysis, Writing – original draft, Writing – review & editing, Visualization. **Viktoria Planz:** Methodology, Validation, Writing – original draft, Writing – review & editing. **Maike Windbergs:** Conceptualization, Resources, Writing – original draft, Writing – review & editing, Supervision, Project administration, Funding acquisition.

Declaration of competing interest

The authors declare the following financial interests/personal

relationships which may be considered as potential competing interests: Maike Windbergs reports financial support was provided by Stiftung zur Förderung der Erforschung von Ersatz- und Ergänzungsmethoden zur Einschränkung von Tierversuchen. Maike Windbergs reports financial support was provided by Deutsche Forschungsgemeinschaft. Maike Windbergs reports financial support was provided by Hessian Ministry for Science and the Arts. Maike Windbergs reports equipment, drugs, or supplies was provided by Agaplesion Markus Krankenhaus, Frankfurt.

Data availability

Data will be made available on request.

Acknowledgements

We thank I. A. Ederer and U. Rieger from Agaplesion Markus Krankenhaus, Frankfurt, Germany for providing excised human skin. Additionally, we would like to thank N. Jung for her scientific input.

Appendix A. Supplementary data

Supplementary data to this article can be found online at https://doi.org/10.1016/j.bioflm.2023.100164.

References

[1] Sen CK. Human wounds and its burden: an updated compendium of estimates. Adv Wound Care 2019;8:39–48. https://doi.org/10.1089/wound.2019.0946.
[2] Malone M, Bjarnsholt T, McBain AJ, James GA, Stoodley P, Leaper D, Tachi M, Schultz G, Swanson T, Wolcott RD. The prevalence of biofilms in chronic wounds: a systematic review and meta-analysis of published data. J Wound Care 2017;26:20–5. https://doi.org/10.12968/jowc.2017.26.1.20.
[3] Wolcott RD, Rhoads DD, Dowd SE. Biofilms and chronic wound inflammation. J Wound Care 2008;17:333–41. https://doi.org/10.12968/jowc.2008.17.8.30796.
[4] Kragh KN, Alhede M, Kvich L, Bjarnsholt T. Into the well-A close look at the complex structures of a microtiter biofilm and the crystal violet assay. Biofilms 2019;1:100006. https://doi.org/10.1016/j.bioflm.2019.100006.
[5] Seth AK, Geringer MR, Hong SJ, Leung KP, Mustoe TA, Galiano RD. In vivo modeling of biofilm-infected wounds: a review. J Surg Res 2012;178:330–8. https://doi.org/10.1016/j.jss.2012.06.048.
[6] Bundesinstitut für Risikobewertung. Verwendung von Versuchstieren im Jahr 2021. 2022.
[7] Mestas J, Hughes CCW. Of mice and not men: differences between mouse and human immunology. J Immunol 2004;172:2731–8. https://doi.org/10.4049/jimmunol.172.5.2731.
[8] Zomer HD, Trentin AG. Skin wound healing in humans and mice: challenges in translational research. J Dermatol Sci 2018;90:3–12. https://doi.org/10.1016/j.jdermsci.2017.12.009.
[9] Steinstraesser L, Sorkin M, Niederbichler AD, Becerikli M, Stupka J, Daigeler A, Kesting MR, Stricker I, Jacobsen F, Schulte M. A novel human skin chamber model to study wound infection ex vivo. Arch Dermatol Res 2010;302:357–65. https://doi.org/10.1007/s00403-009-1009-8.
[10] Coenye T, Kjellerup B, Stoodley P, Bjarnsholt T. The future of biofilm research - report on the '2019 Biofilm Bash'. Biofilms 2020;2:100012. https://doi.org/10.1016/j.bioflm.2019.100012.
[11] Planz V, Lehr C-M, Windbergs M. In vitro models for evaluating safety and efficacy of novel technologies for skin drug delivery. J Contr Release 2016;242:89–104. https://doi.org/10.1016/j.jconrel.2016.09.002.
[12] Kaiser P, Wächter J, Windbergs M. Therapy of infected wounds: overcoming clinical challenges by advanced drug delivery systems, Drug Deliv. Transl Res 2021;11:1545–67. https://doi.org/10.1007/s13346-021-00932-7.
[13] Brackman G, Coenye T. In vitro and in vivo biofilm wound models and their application. Adv Exp Med Biol 2016;897:15–32. https://doi.org/10.1007/5584_2015_5002.
[14] Yoon DJ, Fregoso DR, Nguyen D, Chen V, Strbo N, Fuentes JJ, Tomic-Canic M, Crawford R, Pastar I, Isseroff RR. A tractable, simplified ex vivo human skin model of wound infection. Wound Repair Regen 2019;27:421–5. https://doi.org/10.1111/wrr.12712.
[15] de Breij A, Haisma EM, Rietveld M, El Ghalbzouri A, van den Broek PJ, Dijkshoorn L, Nibbering PH. Three-dimensional human skin equivalent as a tool to study acinetobacter baumannii colonization. Antimicrob Agents Chemother 2012;56:2459–64. https://doi.org/10.1128/AAC.05975-11.
[16] Rancan, Contardi, Jurisch, Blume-Peytavi, Vogt, Bayer, Schaudinn. Evaluation of drug delivery and efficacy of ciprofloxacin-loaded povidone foils and nanofiber mats in a wound-infection model based on ex vivo human skin. Pharmaceutics 2019;11:527. https://doi.org/10.3390/pharmaceutics11100527.
[17] Guzmán-Soto I, McTiernan C, Gonzalez-Gomez M, Ross A, Gupta K, Suuronen EJ, Mah T-F, Griffith M, Alarcon EI. Mimicking biofilm formation and development: recent progress in in vitro and in vivo biofilm models. iScience 2021;24:102443. https://doi.org/10.1016/j.isci.2021.102443.
[18] Shi Di, Mi G, Wang M, Webster TJ. In vitro and ex vivo systems at the forefront of infection modeling and drug discovery. Biomaterials 2019;198:228–49. https://doi.org/10.1016/j.biomaterials.2018.10.030.
[19] Andersson MÅ, Madsen LB, Schmidtchen A, Puthia M. Development of an experimental ex vivo wound model to evaluate antimicrobial efficacy of topical formulations. Int J Mol Sci 2021;22. https://doi.org/10.3390/ijms22095045.
[20] Ashrafi M, Novak-Frazer L, Bates M, Baguneid M, Alonso-Rasgado T, Xia G, Rautemaa-Richardson R, Bayat A. Validation of biofilm formation on human skin wound models and demonstration of clinically translatable bacteria-specific volatile signatures. Sci Rep 2018;8:9431. https://doi.org/10.1038/s41598-018-27504-z.
[21] Brackman G, Cos P, Maes L, Nelis HJ, Coenye T. Quorum sensing inhibitors increase the susceptibility of bacterial biofilms to antibiotics in vitro and in vivo. Antimicrob Agents Chemother 2011;55:2655–61. https://doi.org/10.1128/AAC.00045-11.
[22] Juntke J, Murgia X, Günday Türeli N, Türeli AE, Thorn CR, Schneider M, Schneider-Daum N, de Souza Carvalho-Wodarz C, Lehr C-M. Testing of aerosolized ciprofloxacin nanocarriers on cystic fibrosis airway cells infected with P. aeruginosa biofilms. Drug Deliv. Transl. Res. 2021;11:1752–65. https://doi.org/10.1007/s13346-021-01002-8.
[23] Wächter J, Vestweber PK, Jung N, Windbergs M. Imitating the microenvironment of native biofilms using nanofibrous scaffolds to emulate chronic wound infections. J Mater Chem B 2023;11:3212–25. https://doi.org/10.1039/d2tb02700c.
[24] Sebova K, Bachelor M, Klausner M, Hayden PJ, Oldach J, Stolper G, Li M. A novel assay for evaluating wound healing in a full-thickness in vitro human skin model. Toxicol Lett 2015;238:S185. https://doi.org/10.1016/j.toxlet.2015.08.537.
[25] Toni LS, Garcia AM, Jeffrey DA, Jiang X, Stauffer BL, Miyamoto SD, Sucharov CC. Optimization of phenol-chloroform RNA extraction. MethodsX 2018;5:599–608. https://doi.org/10.1016/j.mex.2018.05.011.
[26] Livak KJ, Schmittgen TD. Analysis of relative gene expression data using real-time quantitative PCR and the 2(-Delta Delta C(T)) Method. Methods 2001;25:402–8. https://doi.org/10.1006/meth.2001.1262.
[27] Tfaili S, Gobinet C, Josse G, Angiboust J-F, Manfait M, Piot O. Confocal Raman microspectroscopy for skin characterization: a comparative study between human skin and pig skin. Analyst 2012;137:3673–82. https://doi.org/10.1039/c2an16292j.
[28] Franzen L, Windbergs M. Applications of Raman spectroscopy in skin research—from skin physiology and diagnosis up to risk assessment and dermal drug delivery. Adv Drug Deliv Rev 2015;89:91–104. https://doi.org/10.1016/j.addr.2015.04.002.
[29] Barry BW, Edwards HGM, Williams AC. Fourier transform Raman and infrared vibrational study of human skin: assignment of spectral bands. J Raman Spectrosc 1992;23:641–5. https://doi.org/10.1002/jrs.1250231113.
[30] Martinez MG, Bullock AJ, MacNeil S, Rehman IU. Characterisation of structural changes in collagen with Raman spectroscopy. Appl Spectrosc Rev 2019;54:509–42. https://doi.org/10.1080/05704928.2018.1506799.
[31] Livak KJ, Schmittgen TD. Analysis of relative gene expression data using real-time quantitative PCR and the 2(-Delta Delta C(T)) Method. Methods 2001;25:402–8. https://doi.org/10.1006/meth.2001.1262.
[32] Vyas HKN, Xia B, Mai-Prochnow A. Clinically relevant in vitro biofilm models: a need to mimic and recapitulate the host environment. Biofilms 2022;4:100069. https://doi.org/10.1016/j.bioflm.2022.100069.
[33] Safferling K, Sütterlin T, Westphal K, Ernst C, Breuhahn K, James M, Jäger D, Halama N, Grabe N. Wound healing revised: a novel reepithelialization mechanism revealed by in vitro and in silico models. J Cell Biol 2013;203:691–709. https://doi.org/10.1083/jcb.201212020.
[34] Shepherd J, Douglas I, Rimmer S, Swanson L, MacNeil S. Development of three-dimensional tissue-engineered models of bacterial infected human skin wounds, Tissue Eng. Part C Methods 2009;15:475–84. https://doi.org/10.1089/ten.tec.2008.0614.
[35] Cicmanec JF, Holder IA. Growth of Pseudomonas aeruginosa in normal and burned skin extract: role of extracellular proteases. Infect Immun 1979;25:477–83. https://doi.org/10.1128/iai.25.2.477-483.1979.
[36] Heck LW, Morihara K, McRae WB, Miller EJ. Specific cleavage of human type III and IV collagens by Pseudomonas aeruginosa elastase. Infect Immun 1986;51:115–8. https://doi.org/10.1128/iai.51.1.115-118.1986.
[37] Gallo RL, Huttner KM. Antimicrobial peptides: an emerging concept in cutaneous biology. J Invest Dermatol 1998;111:739–43. https://doi.org/10.1046/j.1523-1747.1998.00361.x.
[38] Parducho KR, Beadell B, Ybarra TK, Bush M, Escalera E, Trejos AT, Chieng A, Mendez M, Anderson C, Park H, Wang Y, Lu W, Porter E. The antimicrobial peptide human beta-defensin 2 inhibits biofilm production of Pseudomonas aeruginosa without compromising metabolic activity. Front Immunol 2020;11:805. https://doi.org/10.3389/fimmu.2020.00805.
[39] Maisetta G, Batoni G, Esin S, Florio W, Bottai D, Favilli F, Campa M. In vitro bactericidal activity of human beta-defensin 3 against multidrug-resistant nosocomial strains. Antimicrob Agents Chemother 2006;50:806–9. https://doi.org/10.1128/AAC.50.2.806–809.2006.
[40] Bulet P, Stöcklin R, Menin L. Anti-microbial peptides: from invertebrates to vertebrates. Immunol Rev 2004;198:169–84. https://doi.org/10.1111/j.0105-2896.2004.0124.x.
[41] Peschel A. How do bacteria resist human antimicrobial peptides? Trends Microbiol 2002;10:179–86. https://doi.org/10.1016/S0966-842X(02)02333-8.

[42] Percival SL, Thomas JG, Williams DW. Biofilms and bacterial imbalances in chronic wounds: anti-Koch. Int Wound J 2010;7:169–75. https://doi.org/10.1111/j.1742-481X.2010.00668.x.
[43] Hurlow J, Blanz E, Gaddy JA. Clinical investigation of biofilm in non-healing wounds by high resolution microscopy techniques. J Wound Care 2016;25(Suppl 9):S11–22. https://doi.org/10.12968/jowc.2016.25.Sup9.S11.
[44] Kirketerp-Møller K, Jensen PØ, Fazli M, Madsen KG, Pedersen J, Moser C, Tolker-Nielsen T, Høiby N, Givskov M, Bjarnsholt T. Distribution, organization, and ecology of bacteria in chronic wounds. J Clin Microbiol 2008;46:2717–22. https://doi.org/10.1128/JCM.00501-08.
[45] Meduri GU, Kanangat S, Stefan J, Tolley E, Schaberg D. Cytokines IL-1beta, IL-6, and TNF-alpha enhance in vitro growth of bacteria. Am J Respir Crit Care Med 1999;160:961–7. https://doi.org/10.1164/ajrccm.160.3.9807080.
[46] Kaya E, Grassi L, Benedetti A, Maisetta G, Pileggi C, Di Luca M, Batoni G, Esin S. In vitro interaction of Pseudomonas aeruginosa biofilms with human peripheral blood mononuclear cells. Front Cell Infect Microbiol 2020;10:187. https://doi.org/10.3389/fcimb.2020.00187.
[47] Flach CR, Moore DJ. Infrared and Raman imaging spectroscopy of ex vivo skin. Int J Cosmet Sci 2013;35:125–35. https://doi.org/10.1111/ics.12020.
[48] Franzen L, Mathes C, Hansen S, Windbergs M. Advanced chemical imaging and comparison of human and porcine hair follicles for drug delivery by confocal Raman microscopy. J Biomed Opt 2013;18:61210. https://doi.org/10.1117/1.JBO.18.6.061210.
[49] Ali SM, Bonnier F, Lambkin H, Flynn K, McDonagh V, Healy C, Lee TC, Lyng FM, Byrne HJ. A comparison of Raman, FTIR and ATR-FTIR micro spectroscopy for imaging human skin tissue sections. Anal Methods 2013;5:2281. https://doi.org/10.1039/C3AY40185E.
[50] Gröne A. Keratinocytes and cytokines. Vet Immunol Immunopathol 2002;88:1–12. https://doi.org/10.1016/S0165-2427(02)00136-8.
[51] Andonova M, Urumova V. Immune surveillance mechanisms of the skin against the stealth infection strategy of Pseudomonas aeruginosa-review. Comp Immunol Microbiol Infect Dis 2013;36:433–48. https://doi.org/10.1016/j.cimid.2013.03.003.
[52] Zhao G, Usui ML, Lippman SI, James GA, Stewart PS, Fleckman P, Olerud JE. Biofilms and inflammation in chronic wounds. Adv Wound Care 2013;2:389–99. https://doi.org/10.1089/wound.2012.0381.
[53] Grellner W, Georg T, Wilske J. Quantitative analysis of proinflammatory cytokines (IL-1beta, IL-6, TNF-alpha) in human skin wounds. Forensic Sci Int 2000;113:251–64. https://doi.org/10.1016/S0379-0738(00)00218-8.
[54] Galle M, Schotte P, Haegman M, Wullaert A, Yang HJ, Jin S, Beyaert R. The Pseudomonas aeruginosa Type III secretion system plays a dual role in the regulation of caspase-1 mediated IL-1beta maturation. J Cell Mol Med 2008;12:1767–76. https://doi.org/10.1111/j.1582-4934.2007.00190.x.
[55] Liu Y-C, Chan K-G, Chang C-Y. Modulation of host biology by Pseudomonas aeruginosa quorum sensing signal molecules: messengers or traitors. Front Microbiol 2015;6:1226. https://doi.org/10.3389/fmicb.2015.01226.
[56] Marreiro de Sales-Neto J, Lima ÉA, Cavalcante-Silva LHA, Vasconcelos U, Rodrigues-Mascarenhas S. Anti-inflammatory potential of pyocyanin in LPS-stimulated murine macrophages. Immunopharmacol Immunotoxicol 2019;41:102–8. https://doi.org/10.1080/08923973.2018.1555845.
[57] Gabay C. Interleukin-6 and chronic inflammation. Arthritis Res Ther 2006;8(Suppl 2). https://doi.org/10.1186/ar1917. S3.
[58] Johnson BZ, Stevenson AW, Prêle CM, Fear MW, Wood FM. The role of IL-6 in skin fibrosis and cutaneous wound healing. Biomedicines 2020;8. https://doi.org/10.3390/biomedicines8050101.
[59] Baggiolini M, Clark-Lewis I. Interleukin-8, a chemotactic and inflammatory cytokine. FEBS Lett 1992;307:97–101. https://doi.org/10.1016/0014-5793(92)80909-Z.
[60] Schaudinn C, Dittmann C, Jurisch J, Laue M, Günday-Türeli N, Blume-Peytavi U, Vogt A, Rancan F. Development, standardization and testing of a bacterial wound infection model based on ex vivo human skin. PLoS One 2017;12:e0186946. https://doi.org/10.1371/journal.pone.0186946.
[61] Nguyen AV, Soulika AM. The dynamics of the skin's immune system. Int J Mol Sci 2019;20. https://doi.org/10.3390/ijms20081811.
[62] Kirker KR, James GA, Fleckman P, Olerud JE, Stewart PS. Differential effects of planktonic and biofilm MRSA on human fibroblasts. Wound Repair Regen 2012;20:253–61. https://doi.org/10.1111/j.1524-475X.2012.00769.x.
[63] Secor PR, James GA, Fleckman P, Olerud JE, McInnerney K, Stewart PS. Staphylococcus aureus Biofilm and Planktonic cultures differentially impact gene expression, mapk phosphorylation, and cytokine production in human keratinocytes. BMC Microbiol 2011;11:143. https://doi.org/10.1186/1471-2180-11-143.